

## SUPPORTING INFORMATION

*Ren, C., et al.*

### SI MATERIALS and METHODS

**Protein Expression and Purification.** Tandem BRD2/3/4 and single BRD4-BrD constructs were cloned into pNIC28 expression vectors. For protein expression, RIPL-BL21 (DE3)-CodonPlus competent cells transformed with BrD plasmids were grown in TB media at 37°C and switched to 15°C until OD reached approximately 1.8-2.0. Cells were induced by 1 mM isopropyl  $\beta$ -D-1-thiogalactopyranoside (IPTG) for 16-20 hours. Cell paste was collected and lysed in PBS buffer containing 500 mM NaCl and 5% glycerol using microfluidizer. The lysate was centrifuged at 20,000g for 40 mins. Proteins were purified using nickel affinity and Superdex 75 or 200 columns sequentially. His-tag was removed using TEV cleavage after nickel affinity column purification if needed. The purified protein was concentrated in 30 mM HEPES buffer of pH7.4 containing 500 mM ammonium acetate.  $^{15}\text{N}$ -labeled protein was prepared by growing bacterial cells in M9 medium containing  $^{15}\text{N}$ - $\text{NH}_4\text{Cl}$  and the same purification procedure. A list of BrD proteins is in **Table S2**.

**Fluorescence Anisotropy Binding Assay.** The saturation FP assay was performed in the presence of increasing concentrations of BrD proteins.  $K_d$  was determined using one-site saturation binding in GraphPad Prism. The competition FP assay was performed in the presence of BrD protein at larger than  $K_d$  concentration (50%~80% of saturation point) and increasing concentration of compounds. 1% DMSO was consistent among all wells.  $\text{IC}_{50}$  was determined using competition binding fitting  $\text{IC}_{50}$  in GraphPad Prism. The FITC-labeled MS417 (10 nM) (1) was used as an assay probe for both saturation and competition assays.

**Dynamic Light Scattering (DLS) Study.** BRD4 proteins (20  $\mu\text{M}$  tandem BrDs or 40  $\mu\text{M}$  single BrDs) were mixed with monovalent MS417 or JQ1 (40 $\mu\text{M}$ ), or bivalent MS645 or MS660 (20  $\mu\text{M}$ ) (final DMSO concentration was kept at 1%) and separated by Superdex 200 column in the running buffer (30 mM HEPES of pH7.4, 500 mM ammonium acetate) at 0.3 mL/min followed by UV detection and light scattering. Protein Molecular weight calculation was performed using ASTRA® software (Wyatt).

**Protein Crystallization, X-Ray Diffraction Data Collection and Structure Determination.** Purified BRD4-BD1/BD2 (residues 44-477) protein was mixed with MS645 or MS660 at 1:1 molar ratio. The crystallization conditions were listed in **Table S2**. Complex was crystallized via sitting-drop method with equal amounts of protein sample and reservoir solution at 290K. Crystals were mounted using the original crystallization reservoir solution plus 20% ethylene glycol. X-ray diffraction data were collected at 14-1 beamline at the Stanford Synchrotron Radiation Light Source, and processed using CCP4 suite(2). Images were processed using either HKL2000 (3) or iMOSFLM (4). Phase was solved using molecular replacement using BALBES (5). Electron density map refinement, model building and visualization were done using Refmac (6), Phenix refinement (7) and Coot (8). Structure figures were generated using PyMOL Molecular Graphics System (Schrödinger, LLC). The crystallization statistics was listed in **Table S3**.

**NMR Spectroscopy Study.** Protein samples of <sup>15</sup>N-labeled BrDs were prepared in PBS buffer of pH 7.4 containing 10% D<sub>2</sub>O. DMSO was added to help dissolve chemical compounds when needed. The same amount of DMSO was added to the free BrD samples as a control. <sup>1</sup>H-<sup>15</sup>N-HSQC spectra were recorded on Bruker 600Hz or 500Hz NMR spectrometers at 298K. Spectra were processed using NMRPipe (9) and analyzed using NMRViewJ software (10).

**Mutagenesis Study.** BRD4 BD1-BD2 mutants bearing W81A, L92A, L94A, L92A/L94A, N140A, or N433A mutants were generated using QuikChange II XL site-directed mutagenesis kit (Agilent Technologies) following the standard protocol. Mutagenesis primers were designed by <https://www.genomics.agilent.com/primerDesignProgram.jsp>. After the mutant strand was synthesized, DpnI was applied to digest the template. Mutant product was transformed into DH5 $\alpha$  super competent cells (in-house prepared) and positive clones were confirmed by sequencing. Mutants bearing the mutations in both BD1 and BD2 (i.e. N140A/N433A, W81A/W374A, L92A/L94A/L385/387A, or W81A/W374A/L92A/L94A/L385/387A) were generated using the corresponding BD1 mutants as the DNA template following the same procedure.

**Cell Growth Inhibition Assay.** Cells were seeded at 1000 cells per well (for SUM1315 or MCF10A, seed 3000 or 4000 cells per well) in 96-well plate. The next day, cells were treated with compounds starting from 50  $\mu$ M with two-fold dilution (final DMSO concentration 1%) and continued to grow for 4 to 10 days until the wells at the lowest concentration reached full confluency. Next, 20  $\mu$ l 5 mg/mL MTT solution was added directly into medium. Cells were further incubated for at least 4 hours at 37°C. Medium was discarded and 200  $\mu$ l DMSO was added. After the purple precipitants were fully dissolved, absorbance was measured using EnVision® multilabel reader (PerkinElmer) at both 570 nm and 630 nm and calculated as OD570 minus OD630. The IC<sub>50</sub> of growth inhibition was listed in Supplementary Table S4.

**Cellular Thermal Shift Assay.** The assay was performed as previously described (11). MDA-MD-231 cells were treated with increasing amount of cpd and DMSO for 1 hr at 37°C. Later, cells were washed with PBS and heat at 49°C for 3min, left at RT for 3min, and underwent 3 times liquid nitrogen -37°C water-bath cycles. Cell lysate was centrifuged at 16000 g for 30 min and supernatant was collected for western blot analysis with anti-BRD4 (Bethyl A301-985)/goat anti-rabbit IgG-HRP (Santa Cruz sc-2004), anti-beta-Actin (Santa Cruz sc-1616)/bovine anti-goat IgG-HRP (Santa Cruz sc-2350). BRD4 band intensity was normalized to that of DMSO treated samples using Image Studio™ Lite (LI-COR, Inc.).

**Immunoblotting Analysis.** Treated cells were washed with cold PBS and lysed in lysis buffer (Cell Signaling) using a standard protocol. The protein concentration was analyzed by a protein assay kit with bovine serum albumin standards according to the manufacturer's instructions (Bio-Rad Laboratories, Hercules, CA). Cell lysate was separated by SDS-PAGE and transferred onto a nitrocellulose membrane (Hybond-C, Amersham Pharmacia Biotech, Inc., Piscataway, NJ). Following blocking with PBS-Tween-20 containing 5% nonfat dry milk for 1 h, membranes were incubated overnight at 4°C with anti- $\gamma$ -H2AX antibody, anti-cleaved caspase3 antibody, anti-cleaved PARP antibody, anti-CDK4 antibody, anti-CDK6 antibody, anti-CDK2 antibody, anti-Cyclin B1 antibody, anti-CDC2 antibody, anti-P21 antibody, anti-c-Myc antibody, anti-Bax antibody, anti-BCL2 antibody, anti-RAD51 antibody, followed by incubation with

horseradish peroxidase– conjugated secondary antibody.  $\beta$ -actin was used as loading control. All antibodies for experiments were purchased from Cell Signaling Technology. Immunoreactive bands were detected by an enhanced chemiluminescence kit.

**Co-Immunoprecipitation.** Cells were seeded in 10 cm cell culture dish, and then treated with DMSO, 500 nM JQ1 or MS645 the following day for 1 hr. Cells were washed with PBS, lysed in 2 ml Pierce IP Lysis Buffer (ThermoFisher 97788) with protease inhibitor cocktail (Sigma 11836153001) for 1 hr, and centrifuged at 10,000g for 10 min at 4°C. Clear supernatant was harvested and protein concentration was determined using Pierce BCA protein assay reagents (ThermoFisher 23228, 1859228). Protein sample of 1000  $\mu$ g was used for each IP, which was incubated with antibodies (2  $\mu$ g anti-BRD4 Bethyl A301-985; 2  $\mu$ g anti-MED1, Bethyl A300-793A; and 2  $\mu$ g rabbit Santa cruz sc-2027 X) and 25  $\mu$ L of protein G magnetic beads (Dynabeads, Life Technologies) on a LabQuake rotisserie rotator overnight at 4°C. Beads were washed three times with IP lysis buffer and heated at 95°C for 5 min in Laemmli buffer (Biorad) with 2-mercaptoethanol. Eluted co-IP sample and input were separated by SDS-PAGE and transferred onto a PVDF membrane (Millipore IPVH00010) using standard western blot and transfer procedure. Membrane was blocked with 5% fat-free milk for 1 hr at room temperature and incubated with anti-MED1 (Bethyl A300-793A) at 4 °C overnight. After washing three times with TBST, incubating with anti-rabbit-HRP (Santa Cruz sc-2004) for 1hr, membrane was thoroughly washed with TBST and target band was detected using standard chemiluminescent detection with X-ray film.

**Reverse Transcription and Real-Time Quantitative PCR (qPCR).** Total RNA was prepared using TRIzol (Life Technologies) following standard protocol. Reverse transcription was done using SuperScript III reverse transcriptase (Life Technologies). All qPCR assays were performed using SYBR® Premix Ex Taq™ II (Tli RNase H Plus, Clontech). For mRNA transcription analysis, data were normalized to HPRT or GAPDH house-keeping gene and presented as ‘fold change’ between compound and DMSO treated samples. Results were plotted from at least three independent experiments and error bars denoted standard error of the mean (SEM). The primers used in the studies were listed in **Table S2**.

**Transcription Recovery Assay.** Cells were treated with compounds at different concentrations (final DMSO is below 1%) for 2 hours. mRNA extraction, reverse transcription, and qPCR were performed as described above. Primers used for the mRNA detection are in **Table S2**. For the washout study, Cells were pre-treated with 1  $\mu$ M compound for two hours. Medium was removed and cells were washed with 2 ml medium twice to remove the residual compound. Cells were further cultured for 0.5h, 1h, or 2h, and harvest using TRIzol. mRNA extraction, reverse transcription, and qPCR were performed as described above.

**RNA-Seq and Data Analysis.** MDA-MB-231 cells were treated with compounds (final DMSO concentration 1%) for 18 hours. mRNA was extracted using NucleoSpin® RNA (Macherey-Nagel). Library preparation and sequencing (single read) were performed at the Mount Sinai sequencing core facility (sample set 0) and the Epigenomics Core of Weill Cornell Medical College (sample sets 1 and 2). For RNA-Seq data analysis, sequencing short reads were mapped to the reference genome assembly (Hg19) using TopHat (version 2.0.8)(12) and differentially expressed genes were identified using DESeq2(13) . We used the average mean (basemean) of

DMSO sample and 500 nM MS645 sample bigger than 10 as the cutoff to select genes for further analysis (13026 genes, see **Table S4**). Gene clustering was plotted using Multiple Array Viewer (14). Fold change (FC) >2 or <2 was chosen as the cutoff to select genes for Venn diagram analysis and gene enrichment analysis. Venn diagram analysis was performed using Venny (<https://www.stefanjol.nl/venny>) and Venn diagram generator (<http://www.bioinformatics.lu/venn.php>). Enrichment analysis was performed using the Reactome Pathway database (15) integrated in Enrichr (16) (see details in **Table S5**).

**Statistical Analysis.** Statistical analysis was performed using Student's t-Test. P values <0.05 were considered statistically significant.

**Accession codes.** Coordinates and structure factors for the BRD4-BD1 dimer in complex with MS645 or MS660 are deposited in the Protein Data Bank under PDB ID of 6DJC and 6DNE, respectively. All RNA-seq data generated in this study are deposited in the Gene Expression Omnibus under GEO accession code of GSE115550.

**Chemical Synthesis.** Unless otherwise stated, available starting materials were purchased from commercial vendors and used without any further purification. All non-aqueous reactions were carried out in oven-dried glassware under an atmosphere of argon. All solvents were purchased in anhydrous from Acros Organics and used without further purification.

Automatic chromatography was performed on a Biotage Isolera system equipped with a variable wavelength detector and a fraction collector, using Biotage SNAP cartridge KP-Sil 10g. Analytical thin layer chromatography (TLC) was performed employing Sigma-Aldrich 250  $\mu\text{m}$  60F-254 silica plates. The plates were visualized either by exposure to UV light, staining with iodine impregnated silica gel, or by staining with ceric ammonium molybdate (CAM). Preparative TLC was performed employing Silicycle 1000  $\mu\text{m}$  SiliaPlate Prep silica plates. LCMS and HRMS analysis was conducted on an Agilent Technologies G1969A high-resolution API-TOF mass spectrometer attached to an Agilent Technologies 1200 HPLC system. Samples were ionized by electrospray ionization (ESI) in positive mode. Chromatography was performed on a 2.1  $\times$  150 mm Zorbax 300SB-C18 5  $\mu\text{m}$  column with water containing 0.1% formic acid as solvent A and acetonitrile containing 0.1% formic acid as solvent B at a flow rate of 0.4 mL/min. The gradient program was as follows: 1% B (0–1 min), 1–99% B (1–4 min), 99% B (4–8 min). The temperature of the column was held at 50°C for the entire analysis. HPLC purification was carried out on an Agilent 1200 system equipped with a diode array detector (DAD) on a 9.4  $\times$  250 mm Eclipse XDB-C18 5  $\mu\text{m}$  semi-preparative column. The gradient program was as follows: 10% B (0–4 min), 10–90% B (4–14 min), 90% B (14–18 min). NMR spectra were acquired on a Bruker Ascend 400 spectrometer at 400 MHz for  $^1\text{H}$ , a Bruker DRX-600 spectrometer at 600 MHz for  $^1\text{H}$  and 151 MHz for  $^{13}\text{C}$ . Chemical shifts are expressed in parts per million downfield from tetramethylsilane (TMS), using either TMS or the solvent resonance as an internal standard (TMS,  $^1\text{H}$ : 0 ppm; chloroform,  $^{13}\text{C}$ : 77.0 ppm; DMSO- $d_6$ ,  $^1\text{H}$ : 2.50 ppm;  $^{13}\text{C}$ : 39.5 ppm; methanol- $d_4$ ,  $^1\text{H}$ : 3.31 ppm;  $^{13}\text{C}$ : 49.0 ppm). Data are reported as follows: chemical shift, multiplicity (s = singlet, d = doublet, t = triplet, q = quartet, m = multiplet, br = broad), integration, and coupling constant. IR spectra were obtained on a Bruker TENSOR 27 series FT-IR spectrometer equipped with a Diamond ATR. Melting point was measured on an OptiMelt

automatic melting point system MPA100 from Stanford Research System. Optical rotation was measured on an Anton Paar MCP 300 high-precision digital polarimeter.

(S)-MS417 (Methyl (S)-2-(4-(4-chlorophenyl)-2,3,9-trimethyl-6H-thieno[3,2-f][1,2,4]triazolo [4,3-a] [1,4]diazepin-6-yl) acetate) as well as its enantiomer (R)-MS417 were synthesized using a procedure as we reported previously (14) (17). Hydrolysis of (S)-MS417 under lithium hydroxide yielded carboxylic acid **A**. The monomer **A** was coupled to various diamines with diversified linker using standard PyBOP chemistry (**Scheme S1**).

**(S)-2-(4-(4-chlorophenyl)-2,3,9-trimethyl-6H-thieno[3,2-f][1,2,4]triazolo[4,3-a][1,4]diazepin-6-yl)acetic acid (A)**. (S)-MS417 (500 mg, 1.2 mmol, 1.0 equiv) was dissolved in a tetrahydrofuran/water mixture (V/V = 4:1, 15 mL) in a 50 mL round-bottomed flask. To this solution was added lithium hydroxide (577 mg, 24 mmol, 10.0 equiv) dropwise. The mixture was allowed to stir at room temperature for 12 h. After the reaction was complete, the precipitate was filtered under vacuum. The pH of the solution was carefully adjusted to 2 by adding concentrated HCl. The pure product appears as a fine white powder (448 mg, 92%). <sup>1</sup>H NMR (400 MHz, CDCl<sub>3</sub>) δ 7.44 (d, *J* = 8.0 Hz, 2H), 7.35 (d, *J* = 8.4 Hz, 2H), 4.58 (t, *J* = 6.4 Hz, 1H), 3.66-3.61 (m, 2H), 2.70 (s, 3H), 2.42 (s, 3H), 1.70 (s, 3H). MS (*m/z*): calcd for C<sub>19</sub>H<sub>17</sub>ClN<sub>4</sub>O<sub>2</sub>S [M+H]<sup>+</sup>, 401.1; found, 401.1. Purity >95%, *t<sub>R</sub>* = 2.8 min.

**(S)-N,N'-(oxybis(ethane-2,1-diyl))bis(2-((6S)-4-(4-chlorophenyl)-2,3,9-trimethyl-6H-thieno[3,2-f][1,2,4]triazolo[4,3-a][1,4]diazepin-6-yl)acetamide)(1, MS687)**. Following the procedure described in **Scheme S1**, the pure product as a pale yellow powder (60%). <sup>1</sup>H NMR (600 MHz, Methanol-*d*<sub>4</sub>) δ = 8.41 (t, *J* = 4.9 Hz, 2H), 7.43 (d, *J* = 8.5 Hz, 4H), 7.38 (d, *J* = 8.5 Hz, 4H), 4.61 (dd, *J* = 8.9, 5.3 Hz, 2H), 3.61 (t, *J* = 5.5 Hz, 4H), 3.46 (t, *J* = 5.2 Hz, 4H), 3.41 (dd, *J* = 15.2, 8.9 Hz, 4H), 2.68 (s, 6H), 2.43 (s, 6H), 1.68 (s, 6H). HRMS (*m/z*): calcd for C<sub>42</sub>H<sub>43</sub>Cl<sub>2</sub>N<sub>10</sub>O<sub>3</sub>S<sub>2</sub><sup>+</sup> [M+H]<sup>+</sup> 869.2338; found 869.2531. calcd for [M+2H]<sup>2+</sup>/2 435.1208; found 435.1307. Purity >95%, *t<sub>R</sub>* = 5.6 min.

**(S)-N,N'-(1,3-phenylenebis(methylene))bis(2-((6S)-4-(4-chlorophenyl)-2,3,9-trimethyl-6H-thieno[3,2-f][1,2,4]triazolo[4,3-a][1,4]diazepin-6-yl)acetamide) (2, MS688)**. Following a similar procedure as compound **1**, compound **2** was obtained as a pale yellow solid (37%). <sup>1</sup>H NMR (600 MHz, Methanol-*d*<sub>4</sub>) δ = 8.88 (t, *J* = 4.8 Hz, 2H), 7.42–7.39 (m, 1H), 7.36–7.33 (m, 8H), 7.31–7.29 (m, 3H), 4.66 (dd, *J* = 9.0, 5.4 Hz, 2H), 4.54–4.49 (m, 2H), 4.43–4.39 (m, 2H), 3.47 (dd, *J* = 14.9, 9.0 Hz, 2H), 3.35 (dd, *J* = 14.9, 5.4 Hz, 3H), 2.68 (s, 6H), 2.42 (d, *J* = 0.5 Hz, 6H), 1.67 (d, *J* = 0.5 Hz, 6H). HRMS (*m/z*): calcd for C<sub>46</sub>H<sub>43</sub>Cl<sub>2</sub>N<sub>10</sub>O<sub>2</sub>S<sub>2</sub><sup>+</sup> [M+H]<sup>+</sup> 901.2389; found 901.2279. Purity >95%, *t<sub>R</sub>* = 5.6 min.

**(S)-N,N'-((ethane-1,2-diylbis(oxy))bis(ethane-2,1-diyl))bis(2-((6S)-4-(4-chlorophenyl)-2,3,9-trimethyl-6H-thieno[3,2-f][1,2,4]triazolo[4,3-a][1,4]diazepin-6-yl)acetamide) (3, MS660)**. Following a similar procedure as compound **1**, compound **3** was obtained as a pale yellow solid (36%). <sup>1</sup>H NMR (600 MHz, Methanol-*d*<sub>4</sub>) δ = 8.41 (t, *J* = 4.9 Hz, 2H), 7.43 (d, *J* = 8.4 Hz, 4H), 7.37 (d, *J* = 8.8 Hz, 4H), 4.61 (dd, *J* = 8.9, 5.3 Hz, 2H), 3.67 (s, 4H), 3.62 (dt, *J* = 5.4, 1.2 Hz, 4H), 3.46 (t, *J* = 5.2 Hz, 2H), 3.41 (dd, *J* = 15.1, 8.9 Hz, 2H), 2.68 (s, 6H), 2.43 (s, 6H), 1.68 (s, 6H). HRMS (*m/z*): calcd for C<sub>44</sub>H<sub>47</sub>Cl<sub>2</sub>N<sub>10</sub>O<sub>4</sub>S<sub>2</sub><sup>+</sup> [M+H]<sup>+</sup> 913.2600; found 913.2586. Purity >97%, *t<sub>R</sub>* = 5.5 min.

**(S)-N,N'-(((oxybis(ethane-2,1-diyl))bis(oxy))bis(ethane-2,1-diyl))bis(2-((6S)-4-(4-chlorophenyl)-2,3,9-trimethyl-6H-thieno[3,2-f][1,2,4]triazolo[4,3-a][1,4]diazepin-6-yl)acetamide) (4, MS661).** Following a similar procedure as compound **1**, compound **4** was obtained as a pale yellow solid (47%). <sup>1</sup>H NMR (600 MHz, Methanol-*d*<sub>4</sub>) δ = 8.41 (br s, 2H), 7.43 (d, *J* = 8.5 Hz, 4H), 7.38 (d, *J* = 8.5 Hz, 4H), 4.61 (dd, *J* = 9.0, 5.2 Hz, 2H), 3.69–3.64 (m, 10H), 3.62 (dt, *J* = 5.5, 1.4 Hz, 4H), 3.49–3.41 (m, 6H), 2.68 (s, 6H), 2.43 (s, 6H), 1.67 (s, 6H). HRMS (m/z): calcd for C<sub>46</sub>H<sub>51</sub>Cl<sub>2</sub>N<sub>10</sub>O<sub>5</sub>S<sub>2</sub><sup>+</sup> [M+H]<sup>+</sup> 957.2862; found 957.2018. calcd for C<sub>23</sub>H<sub>26</sub>ClN<sub>5</sub>O<sub>5</sub>S<sup>+</sup> [M+2H]<sup>2+</sup>/2 479.1471; found 479.1245. Purity >97%, t<sub>R</sub> = 5.6 min.

**(S)-N,N'-(decane-1,10-diyl)bis(2-((6S)-4-(4-chlorophenyl)-2,3,9-trimethyl-6H-thieno[3,2-f][1,2,4]triazolo[4,3-a][1,4]diazepin-6-yl)acetamide) (5, MS645).** Following a similar procedure as compound **1**, compound **5** was obtained as a pale yellow solid (51%). <sup>1</sup>H NMR (600 MHz, Methanol-*d*<sub>4</sub>) δ = 8.33 (t, *J* = 5.5 Hz, 2H), 7.45 (d, *J* = 8.5 Hz, 4H), 7.39 (d, *J* = 8.8 Hz, 4H), 4.62 (dd, *J* = 9.2, 5.0 Hz, 2H), 3.41 (dd, *J* = 14.8, 9.2 Hz, 2H), 3.29–3.19 (m, 6H), 2.69 (s, 6H), 2.44 (s, 6H), 1.70 (s, 6H), 1.56 (dt, *J* = 14.5, 7.2 Hz, 4H), 1.39–1.27 (m, 12H). HRMS (m/z): calcd for C<sub>48</sub>H<sub>55</sub>Cl<sub>2</sub>N<sub>10</sub>O<sub>2</sub>S<sub>2</sub><sup>+</sup> [M+H]<sup>+</sup> 937.3328; found 936.2473. calcd for C<sub>24</sub>H<sub>28</sub>ClN<sub>5</sub>OS<sup>+</sup> [M+2H]<sup>2+</sup>/2 469.1703; found 469.1584. Purity >97%, t<sub>R</sub> = 6.0 min.

**(S)-N,N'-(dodecane-1,12-diyl)bis(2-((6S)-4-(4-chlorophenyl)-2,3,9-trimethyl-6H-thieno[3,2-f][1,2,4]triazolo[4,3-a][1,4]diazepin-6-yl)acetamide) (6, MS659).** Following a similar procedure as compound **1**, compound **6** was obtained as a pale yellow solid (47%). <sup>1</sup>H NMR (600 MHz, Methanol-*d*<sub>4</sub>) δ = 8.34 (t, *J* = 5.5 Hz, 2H), 7.45 (d, *J* = 8.5 Hz, 4H), 7.39 (d, *J* = 8.8 Hz, 4H), 4.62 (dd, *J* = 9.2, 5.0 Hz, 2H), 3.41 (dd, *J* = 14.8, 9.3 Hz, 2H), 3.29–3.19 (m, 6H), 2.69 (s, 6H), 2.44 (s, 6H), 1.70 (s, 6H), 1.56 (quintet, *J* = 7.2 Hz, 5H), 1.37–1.29 (m, 16H). HRMS (m/z): calcd for C<sub>50</sub>H<sub>59</sub>Cl<sub>2</sub>N<sub>10</sub>O<sub>2</sub>S<sub>2</sub><sup>+</sup> [M+H]<sup>+</sup> 965.3641; found 965.3239. calcd for C<sub>25</sub>H<sub>30</sub>ClN<sub>5</sub>OS<sup>+</sup> [M+2H]<sup>2+</sup>/2 483.1860; found 483.1933. Purity >97%, t<sub>R</sub> = 6.4 min.

**N-(2-(2-(2-aminoethoxy)ethoxy)ethyl)-2-((6S)-4-(4-chlorophenyl)-2,3,9-trimethyl-6H-thieno[3,2-f][1,2,4]triazolo[4,3-a][1,4]diazepin-6-yl)acetamide (7, MS689).** Following a similar procedure as compound **1**, compound **7** was obtained as a pale yellow solid (15%). <sup>1</sup>H NMR (600 MHz, Methanol-*d*<sub>4</sub>) δ = 8.46 (t, *J* = 6.0 Hz, 2H), 7.46 (d, *J* = 8.5 Hz, 2H), 7.42 (d, *J* = 8.8 Hz, 2H), 4.63 (t, *J* = 4.4 Hz, 1H), 3.66–3.60 (m, 4H), 3.54 (t, *J* = 5.6 Hz, 2H), 3.48–3.41 (m, 4H), 3.34 (t, *J* = 5.5 Hz, 2H), 2.70 (s, 3H), 2.45 (s, 3H), 1.92 (s, 3H), 1.70 (s, 3H). HRMS (m/z): calcd for C<sub>25</sub>H<sub>32</sub>ClN<sub>6</sub>O<sub>3</sub>S<sup>+</sup> [M+H]<sup>+</sup> 531.1935; found 531.2034. Purity >97%, t<sub>R</sub> = 4.9 min.

**(R)-N,N'-(decane-1,10-diyl)bis(2-((6R)-4-(4-chlorophenyl)-2,3,9-trimethyl-6H-thieno[3,2-f][1,2,4]triazolo[4,3-a][1,4]diazepin-6-yl)acetamide) (8, MS993).** (R)-MS417 was synthesized using a procedure as we previously reported (14), and used to generate R-enantiomer of compound **A**, as described above. Following a similar procedure as compound **1**, compound **8** was obtained as a pale yellow solid (60%). <sup>1</sup>H NMR (400 MHz, CDCl<sub>3</sub>) δ 7.41 (d, *J* = 7.6 Hz, 4H), 7.33 (d, *J* = 8.0 Hz, 4H), 6.64 (s, 2H), 4.65 (t, *J* = 12.8 Hz, 2H), 3.56 (dd, *J* = 14.4 Hz, 7.2 Hz, 2H), 3.40–3.34 (dd, *J* = 14.4 Hz, 6.8 Hz, 2H), 3.28 (dt, *J* = 13.6 Hz, 7.2 Hz, 4H), 2.68 (s, 6H), 2.41 (s, 6H), 1.67 (s, 6H), 1.54 (m, 4H), 1.27 (d, *J* = 12.0 Hz, 12H). MS (m/z): calcd for C<sub>48</sub>H<sub>54</sub>Cl<sub>2</sub>N<sub>10</sub>O<sub>2</sub>S<sub>2</sub> [M+H]<sup>+</sup>, 937.3; found, 937.3. Purity >95%, t<sub>R</sub> = 3.0 min.

**2-((R)-4-(4-chlorophenyl)-2,3,9-trimethyl-6H-thieno[3,2-f][1,2,4]triazolo[4,3-a][1,4]diazepin-6-yl)-N-(10-(2-((S)-4-(4-chlorophenyl)-2,3,9-trimethyl-6H-thieno[3,2-f][1,2,4]triazolo[4,3-a][1,4]diazepin-6-yl)acetamido)decyl)acetamide (9, MS994).** Following a similar procedure as compound **8**, compound **9** was obtained as a pale yellow solid (60%). <sup>1</sup>H NMR (400 MHz, CDCl<sub>3</sub>) δ 7.41 (d, *J* = 8.0 Hz, 4H), 7.33 (d, *J* = 8.0 Hz, 4H), 6.51 (s, 2H), 4.63 (t, *J* = 12.0 Hz, 2H), 3.55 (dd, *J* = 12.0 Hz, 8.0 Hz, 2H), 3.34 (dd, *J* = 14.4 Hz, 6.8 Hz, 4H), 3.28 (dd, *J* = 13.6 Hz, 7.2 Hz, 2H), 2.68 (s, 6H), 2.40 (s, 6H), 1.67 (s, 6H), 1.53-1.50 (m, 4H), 1.27 (d, *J* = 11.6 Hz, 12H). MS (m/z): calcd for C<sub>48</sub>H<sub>54</sub>Cl<sub>2</sub>N<sub>10</sub>O<sub>2</sub>S<sub>2</sub> [M+H]<sup>+</sup>, 937.3; found, 937.3. Purity >95%, t<sub>R</sub> = 2.2 min.

**N,N'-(3,6,9,12,15,18,21-heptaotricosane-1,23-diyl)bis(2-((S)-4-(4-chlorophenyl)-2,3,9-trimethyl-6H-thieno[3,2-f][1,2,4]triazolo[4,3-a][1,4]diazepin-6-yl)acetamide) (10, MT1)** (18). Following a similar procedure as compound **1**, compound **10** was obtained as a white solid (57.7%). <sup>1</sup>H NMR (400 MHz, DMSO-d<sub>6</sub>) δ 1.61 (s, 6H), 2.40 (s, 6H), 2.58 (s, 6H), 3.15-3.30 (m, 8H), 3.43-3.68 (m, 28H), 4.41-4.57 (m, 2H), 7.42 (s, 4H), 7.45-7.56 (m, 4H), 8.18-8.42 (m, 2H). MS (m/z): calcd for C<sub>54</sub>H<sub>66</sub>Cl<sub>2</sub>N<sub>10</sub>O<sub>9</sub>S<sub>2</sub> [M+H]<sup>+</sup> 1133.3; found: 1133.3. Purity >98%, t<sub>R</sub> = 2.98 min.

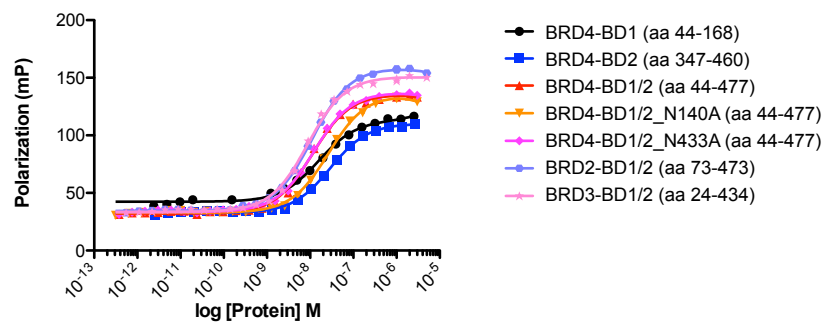
## References:

1. Zhang GT, *et al.* (2012) Down-regulation of NF-kappa B Transcriptional Activity in HIV-associated Kidney Disease by BRD4 Inhibition. *Journal of Biological Chemistry* 287(34):28840-28851.
2. Winn MD, *et al.* (2011) Overview of the CCP4 suite and current developments. *Acta Crystallogr D Biol Crystallogr* 67(Pt 4):235-242.
3. Otwinowski Z & Minor W (1997) Processing of X-ray diffraction data collected in oscillation mode. *Method Enzymol* 276:307-326.
4. Battye TGG, Kontogiannis L, Johnson O, Powell HR, & Leslie AGW (2011) iMOSFLM: a new graphical interface for diffraction-image processing with MOSFLM. *Acta Crystallogr D* 67:271-281.
5. Long F, Vagin AA, Young P, & Murshudov GN (2008) BALBES: a molecular-replacement pipeline. *Acta Crystallogr D Biol Crystallogr* 64(Pt 1):125-132.
6. Murshudov GN, Vagin AA, & Dodson EJ (1997) Refinement of macromolecular structures by the maximum-likelihood method. *Acta Crystallogr D* 53:240-255.
7. Adams PD, *et al.* (2010) PHENIX: a comprehensive Python-based system for macromolecular structure solution. *Acta Crystallogr D* 66:213-221.
8. Emsley P & Cowtan K (2004) Coot: model-building tools for molecular graphics. *Acta Crystallogr D Biol Crystallogr* 60(Pt 12 Pt 1):2126-2132.
9. Delaglio F, *et al.* (1995) Nmrpipe - a Multidimensional Spectral Processing System Based on Unix Pipes. *Journal of Biomolecular Nmr* 6(3):277-293.
10. Johnson BA (2004) Using NMRView to visualize and analyze the NMR spectra of macromolecules. *Methods in molecular biology* 278:313-352.
11. Molina DM, *et al.* (2013) Monitoring Drug Target Engagement in Cells and Tissues Using the Cellular Thermal Shift Assay. *Science* 341(6141):84-87.
12. Trapnell C, Pachter L, & Salzberg SL (2009) TopHat: discovering splice junctions with RNA-Seq. *Bioinformatics* 25(9):1105-1111.
13. Anders S & Huber W (2010) Differential expression analysis for sequence count data. *Genome Biol* 11(10):R106.
14. Saeed AI, *et al.* (2003) TM4: a free, open-source system for microarray data management and analysis. *BioTechniques* 34(2):374-378.
15. Fabregat A, *et al.* (2016) The Reactome pathway Knowledgebase. *Nucleic Acids Res* 44(D1):D481-487.



16. Kuleshov MV, *et al.* (2016) Enrichr: a comprehensive gene set enrichment analysis web server 2016 update. *Nucleic Acids Res* 44(W1):W90-97.
17. Zhang G, *et al.* (2013) Structure-Guided Design of Potent Diazobenzene Inhibitors for the BET Bromodomains. *J. Med. Chem.* 56:9251-9264.
18. Tanaka M, *et al.* (2016) Design and characterization of bivalent BET inhibitors. *Nat Chem Biol* 12(12):1089-1096.

**A** Saturation Binding of FITC-MS417 to BET BrD Proteins



BET BrD Proteins	$K_D$ (nM)	Protein used in competition FP assay (nM)
BRD4-BD1 (aa 44-168)	15.6	46.0
BRD4-BD2 (aa 347-460)	29.1	80.0
BRD4-BD1/2 (aa 44-477)	11.4	20.0
BRD4-BD1/2_N140A (aa 44-477)	27.2	42.0
BRD4-BD1/2_N433A (aa 44-477)	12.1	24.0
BRD2-BD1/2 (aa 73-473)	11.1	17.0
BRD3-BD1/2 (aa 24-434)	8.8	17.0

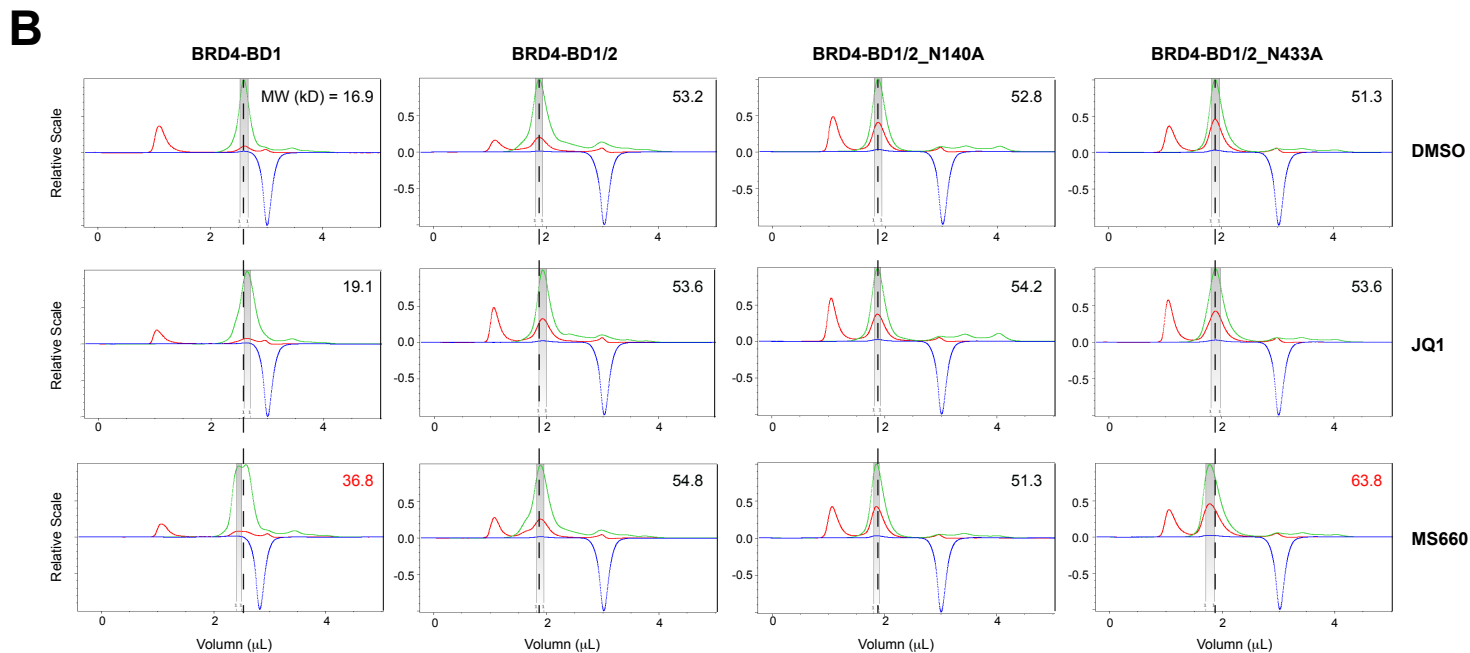
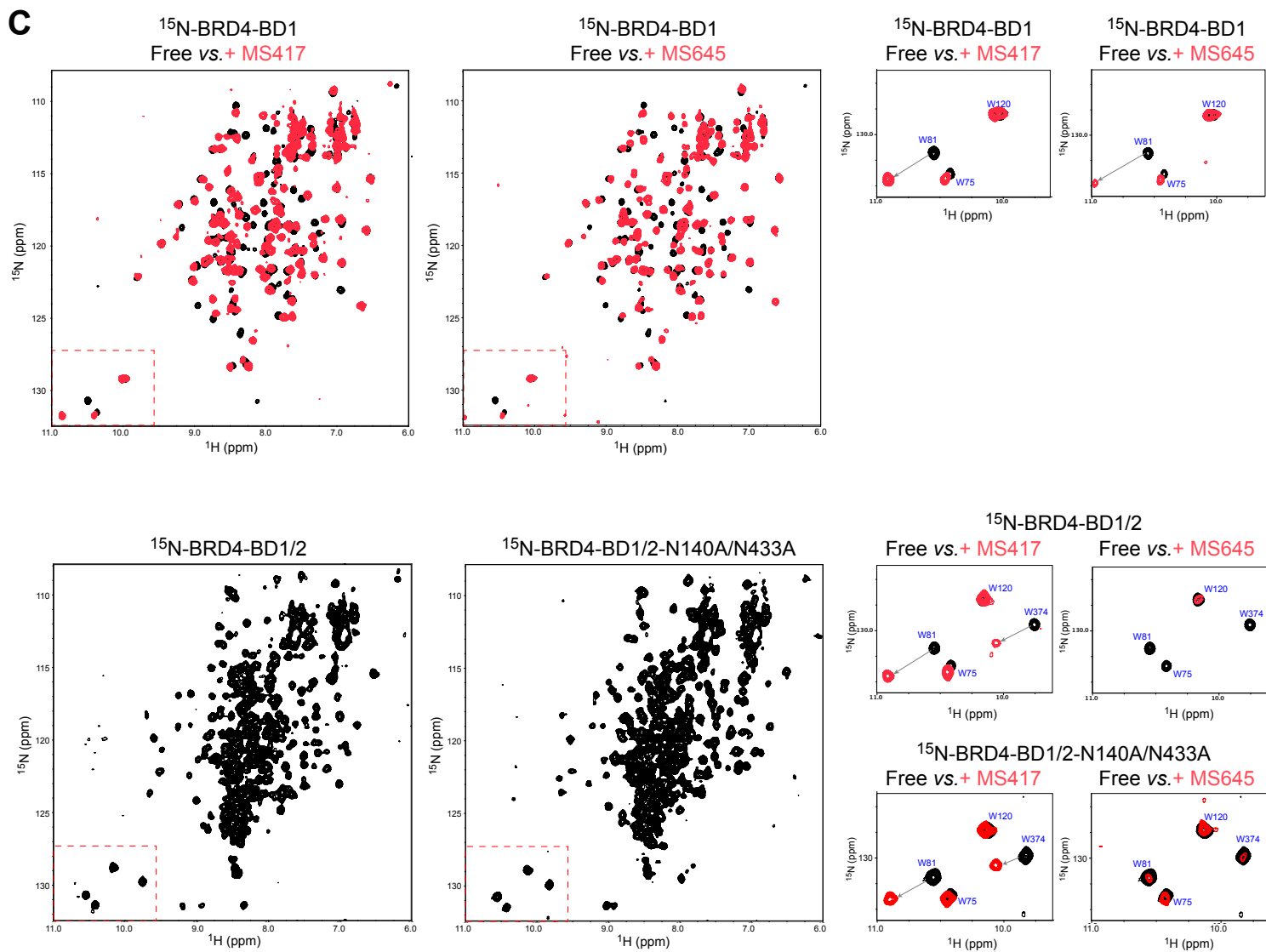
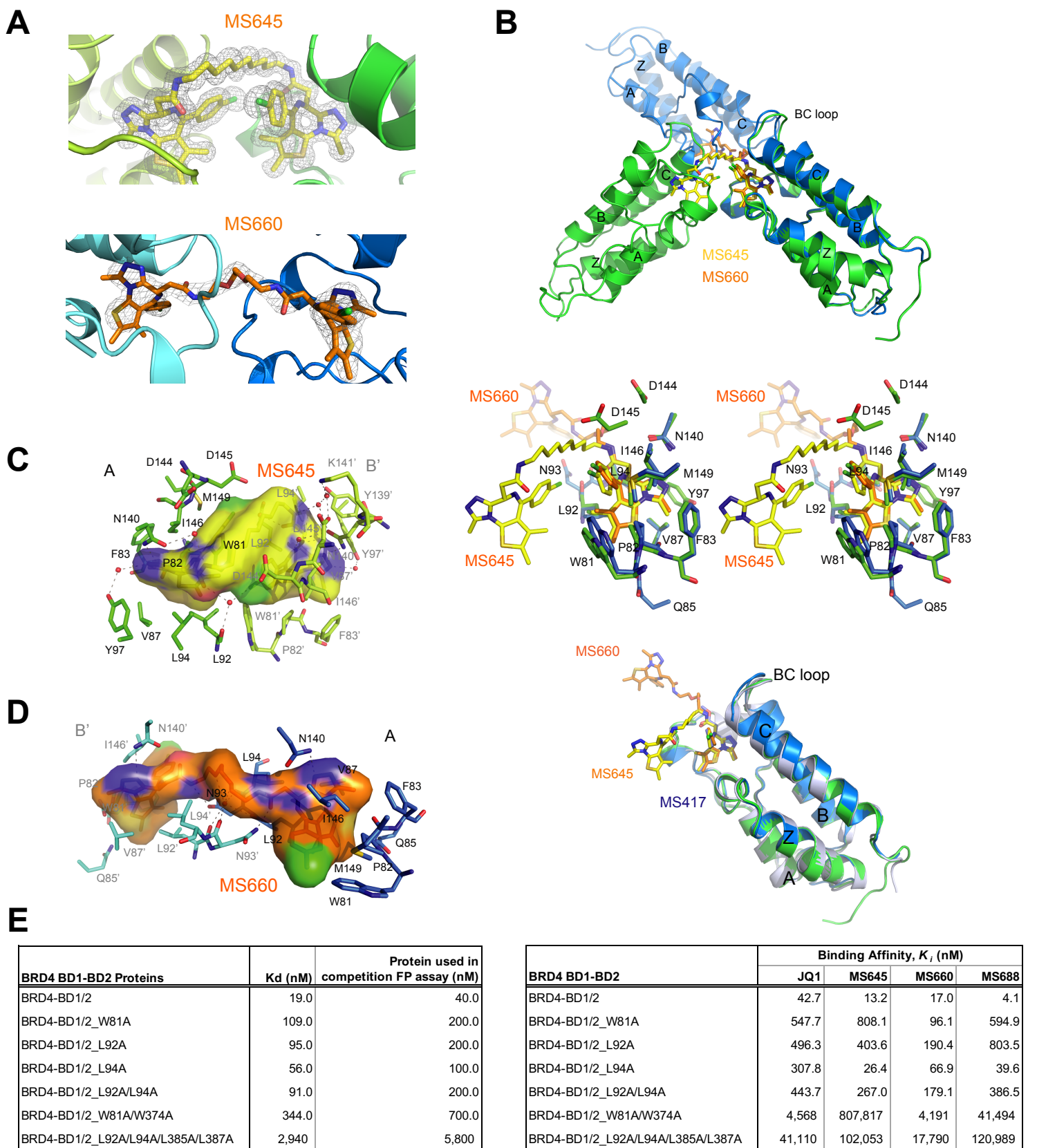


Fig. S1 (continued)



**Fig. S1.** Biophysical characterization of bivalent BrD inhibition of the BET proteins. (A) Binding affinity of FITC-MS417 (MS574), as an assay probe to various BET BrD proteins used in this study, as determined by using a saturation fluorescence polarization (FP) assay.  $K_d$  was determined using GraphPad Prism. (B) Effects of BrD inhibitor binding on protein conformation of BRD4 BD1 alone or tandem BD1/BD2, as assessed by apparent molecular weight of the protein determined by dynamic light scattering (DLS). Measurements of UV, scattering intensity and refractive index change are color-coded in green, red, and blue, respectively. (C) Comparison of monovalent and bivalent BrD inhibitors' binding to BRD4 BD1 alone or tandem BD1/BD2 as illustrated by changes of backbone amide resonances in 2D  $^1\text{H}$ - $^{15}\text{N}$  HSQC of the protein. NMR signals of the BRD4 BD1 and tandem BD1-BD2 wild-type proteins or BD1/BD2-N140A/N433A mutant protein in free form and in presence of a BrD inhibitor MS417 or MS645 are depicted in black and red, respectively. Side-chain indole NH signals of Trp residues shown highlight NMR resonance perturbation and/or line broadening induced by the BrD inhibitor binding.



**Fig. S2.** Structural insights into bivalent BrD inhibitor binding to BRD4. (A) Sigma-A weighted 2mFo-DFc map, depicting the electron density of MS645 (left) and MS660 (right) in the BRD4 BD1 dimer. *Lower panel*, comparison of crystal structures of the BD1 bound to MS645 (yellow), or MS660 (orange). (B) Comparison of domain-domain orientation of the BD1 dimer (colored in green and blue, respectively) when bound to MS645 or MS660. Middle panel, stereo-view of crystal structures of the BD1 bound to MS645 (yellow), or MS660 (orange). Lower panel, stereo-view of BD1 recognition of bivalent MS645 and MS660 vs. monovalent MS417. (C), (D) Space-filled depiction of MS645 or MS660 recognition by the BRD4 BD1 dimer. *Note* that residues from the symmetry-related monomer in the BD1 dimer are colored with lighter green or blue and annotated with '. Hydrogen bonds are shown as dashes. (E) Left panel, binding affinity of FITC-MS417 (MS574), as an assay probe to the various BRD4 BD1-BD2 proteins used in this study, as determined using a saturation FP assay.  $K_d$  was determined using GraphPad Prism. Right panel, binding affinity of the BET BrD inhibitors to the BRD4 BD1-BD2 wild-type and mutant proteins, as determined by the FP competition binding assay.

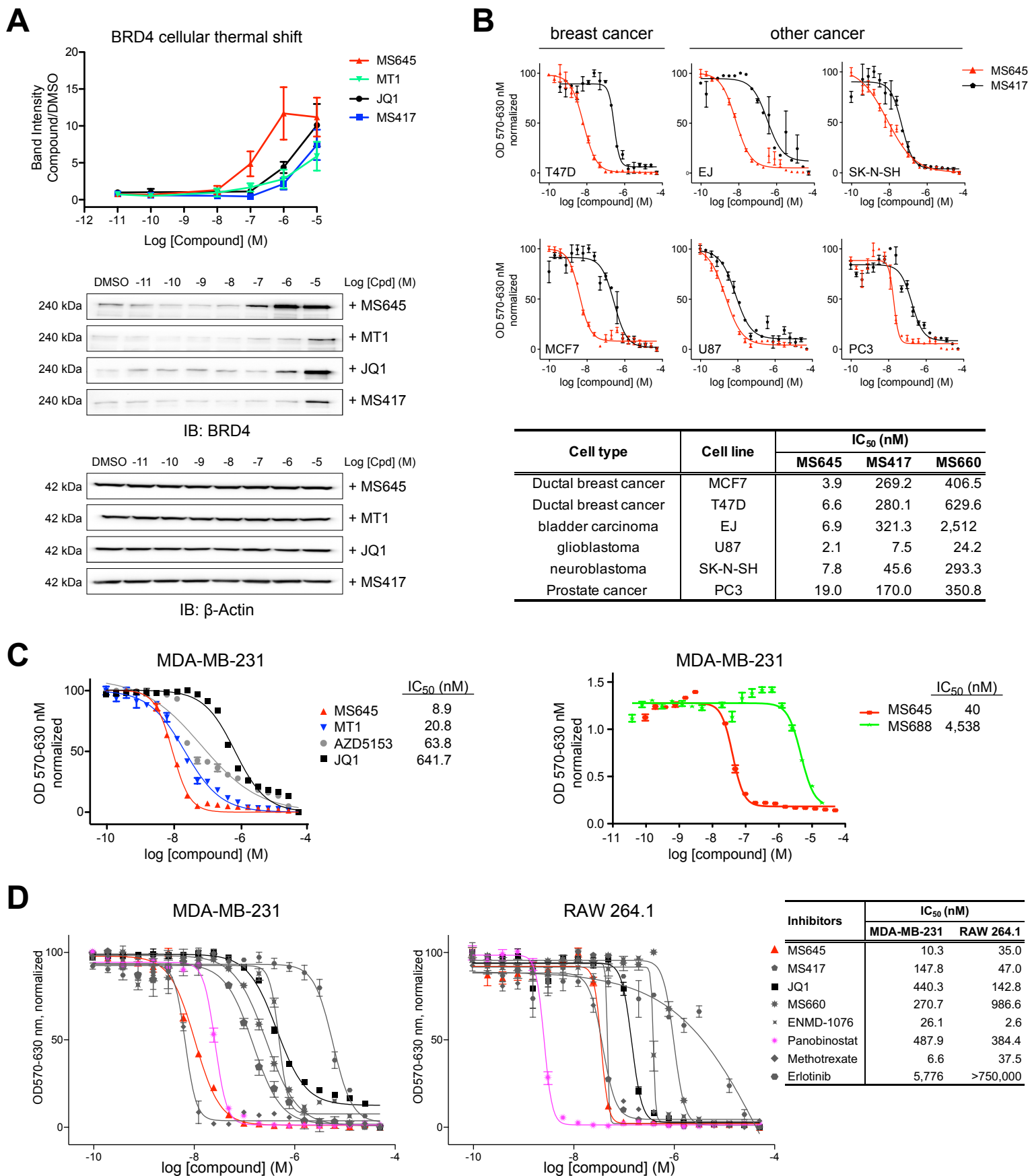


**Fig. S3.** Comparison of cellular activities of MS645 and other small molecule inhibitors. (A) Effects of MS645, MT1, JQ1 and MS417 on BRD4 stability in HEK293T cells, as assessed by a cellular thermal shift assay. (B) Effects of MS645, MS660, JQ1 and MS417 on cell growth inhibition of different cancer cell lines, as assessed in a MTT assay. (C) Effects of MS645 vs. MT1, AZD5153, and JQ1 (left plot), as well as MS645 vs. MS688 (right plot) on cell growth inhibition of MDA-MB-231 TNBC cells, as assessed in a MTT assay. (D) Effects of the BET BrD inhibitors of MS645, MS660, JQ1 and MS417 and various available cancer drugs on cell growth inhibition of MDA-MB-231 cells and macrophage RAW 264.1 cells, as assessed in the MTT assay. All results presented represent at least three independent experiments, and error bars donated standard error of the mean (S.E.M.). IC<sub>50</sub> values are listed in an insert.

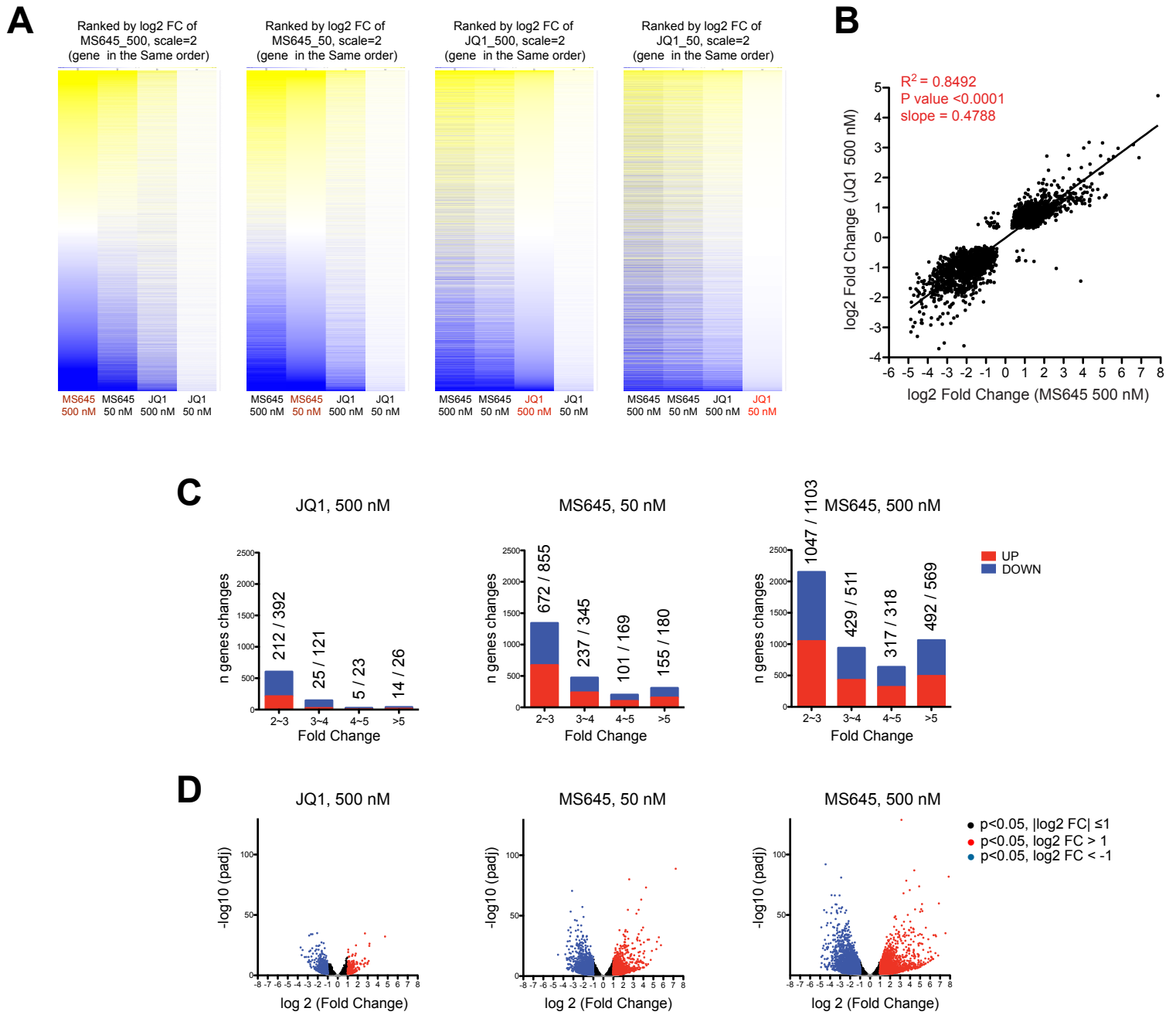
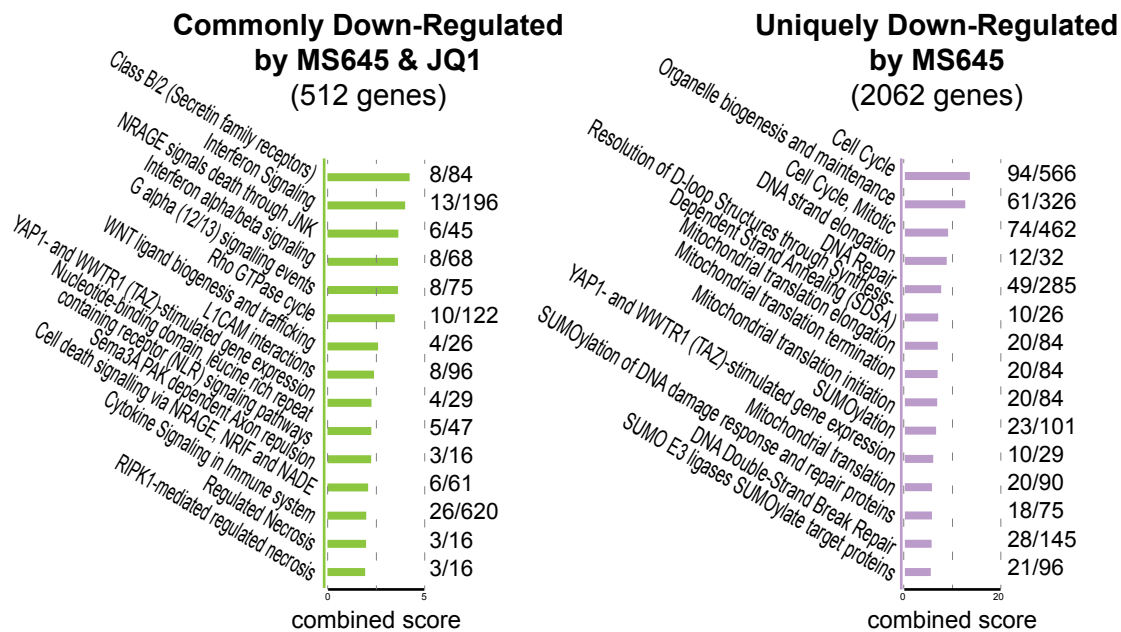
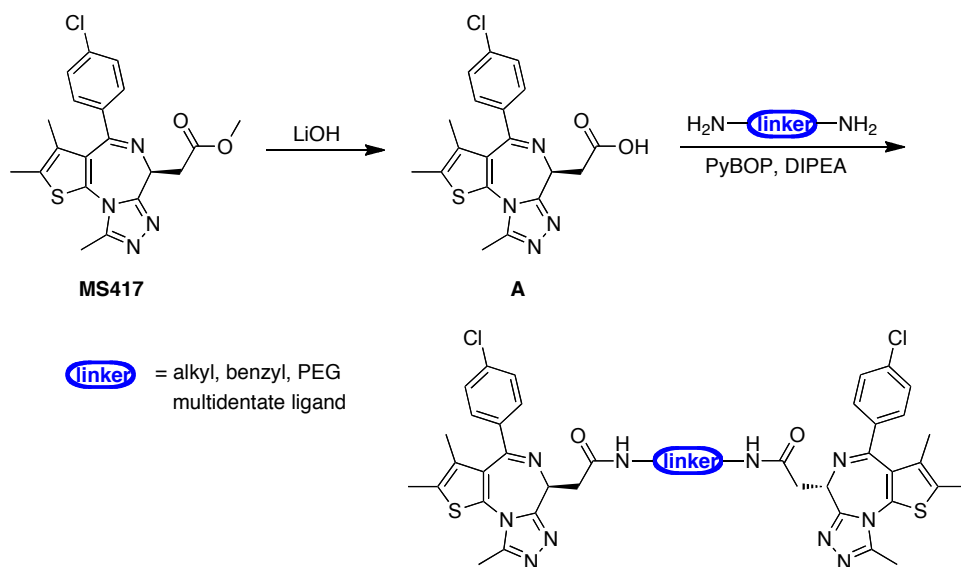


Fig. S4. (continued)

**E**

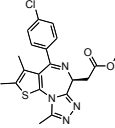
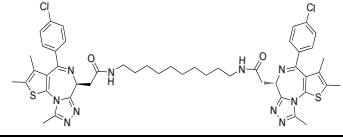
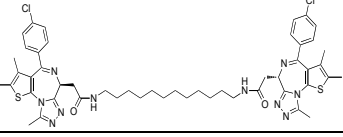
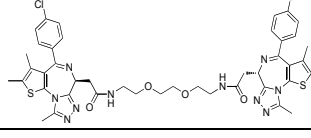
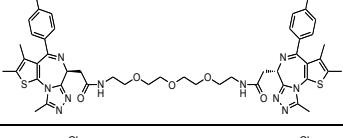
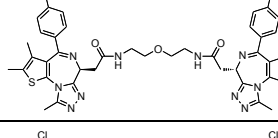
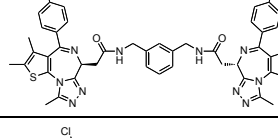
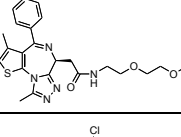
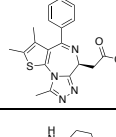
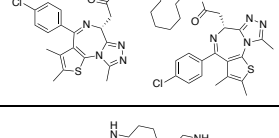
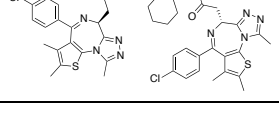
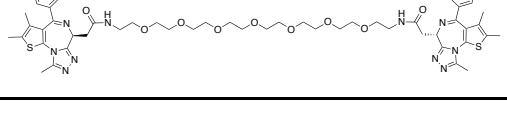
**Fig. S4.** Genomic analysis of gene transcriptional modulation by MS645 vs. JQ1. (A) Global changes in gene transcription of MDA-MB-231 cells treated with MS645 or JQ1 at 50 or 500 nM, respectively, as shown in log2 fold change scale. mRNA was collected for RNA-seq analysis from the MDA-MB-231 cells after treatment of DMSO, MS645, or JQ1 for 18 hours. (B) Scatterplot depicts the analysis only for genes significantly affected by both JQ1 and MS645. There are many more genes affected by MS645 only. Note that the log-scale linear correlation indicates the difference of Fold Change in an exponential manner. (C) The total number of protein coding genes significantly up- or downregulated by JQ1 (500 nM) or MS645 (50 or 500 nM) for 18 hrs were categorized into four groups based on their mean fold change compared to the untreated samples. The number of up-regulated genes was divided by the number of down-regulated genes in each expression group as displayed in the percentage ratio. (D) Volcano plot of gene expression differences between treated and non-treated samples. Color-coded dots highlight all the statistically significant downregulated/upregulated transcripts, as indicated on right. (E) Gene enrichment analysis of genes down-regulated by MS645 (50nM and 500 nM) and JQ1 (500 nM) treatment. The bar length indicated the combined score of particular enriched category and only the top 15 categories from the enrichment analysis were shown.



**Scheme S1.** Synthetic scheme of bivalent BET bromodomain inhibitors



**Table S1. List of BET bromodomain inhibitor compounds**

Compound	Structure	Linker Type
MS417		
MS645		alkyl-linker
MS659		
MS660		PEG-linker
MS661		
MS687		
MS688		benzene-linker
MS689		MS417+tail
Compound A		
MS993		alkyl-linker
MS994		alkyl-linker
MT1		PEG-linker

**Table S2. List of Bromodomain proteins, crystallization conditions, and primers in the study**

Name	Synonym	Application	Vector	Cleavage
BRD4-BD1 (aa 44-168)	BRD4 bromodomain 1	FP, HSQC, DLS	pNIC28	TEV
BRD4-BD2 (aa 347-460)	BRD4 bromodomain 2	FP, HSQC	pNIC28	TEV
BRD4-BD1/2 (aa 44-477)	BRD4 bromodomain 1, linker region & bromodomain 2	FP, HSQC, DLS, Crystallization	pNIC28	TEV
BRD2-BD1/2 (aa 73-473)	BRD2 bromodomain 1, linker region & bromodomain 2	FP	pNIC28	TEV
BRD3-BD1/2 (aa 24-434)	BRD3 bromodomain 1, linker region & bromodomain 2	FP	pNIC28	TEV
BRD4-BD1/2_N140A (aa 44-477)	tandem BRD4 BD1 mutant	FP, HSQC, DLS	pNIC28	TEV
BRD4-BD1/2_N433A (aa 44-477)	tandem BRD4 BD2 mutant	FP, HSQC, DLS	pNIC28	TEV
BRD4-BD1/2_N140A/N433A (aa 44-477)	tandem BRD4 double mutant	FP, HSQC	pNIC28	TEV
BRD4-BD1/2_W81A (aa 44-477)	tandem BRD4 BD1/BD2 mutant	FP	pNIC28	TEV
BRD4-BD1/2_L92A (aa 44-477)	tandem BRD4 BD1/BD2 mutant	FP	pNIC28	TEV
BRD4-BD1/2_L94A (aa 44-477)	tandem BRD4 BD1/BD2 mutant	FP	pNIC28	TEV
BRD4-BD1/2_L92A/L94A (aa 44-477)	tandem BRD4 BD1/BD2 mutant	FP	pNIC28	TEV
BRD4-BD1/2_W81A/W374A (aa 44-477)	tandem BRD4 BD1/BD2 mutant	FP	pNIC28	TEV
BRD4-BD1/2_L92A/L94A/W81A/W374A (aa 44-477)	tandem BRD4 BD1/BD2 mutant	FP	pNIC28	TEV
Crystal complex	Ratio	Crystallization condition	Cryo reagent	Presence in unit cell
BRD4-BD1/2-MS645	0.35 mM BRD4-BD1/2 : 0.35 mM MS645	0.2 M Ammonium Sulfate, 0.1 M Bis-Tris pH 6.5, 25% w/v PEG 3350	20% Ethelene Glycol	2 x BRD4-BD1 - 1 x MS645
BRD4-BD1/2-MS660	0.5 mM BRD4-BD1/2 : 0.5 mM MS660	30% PEG 4000, 0.1 M Tris HCl pH 8.5, 0.2 M Magnesium Chloride	20% Ethelene Glycol	2 x BRD4-BD1 - 1 x MS660
Primers for mRNA-qPCR	Forward	Reverse		
IL6	TCTCCACAATTCGGTCCAGTT	CAACACCAGGAGCAGCCC		
HPRT	GCTATAAATCTTTGCTGACCTGCTG	AATTACTTTTATGTCCCCTGTTGACTGG		
GAPDH	ACCACAGTCCATGCCATCAC	TCCACCACCCTGTTGCTGT		
RXRA	ACCCACCCTGGGCTTCA	ATAGTGCTTGCCTGAGGAGC		
MRPL9	TAGTTGCCCGCCACTTCTTT	AGCCCATTTACCGTCACCTC		
NUP107	GCCTTTTACCCCAACAAGCC	CTGTGTTTGTGAACAGCCCG		
RFC4	ACGAGAAGCCAGGCTAACTG	TTGGGCGATATTTTCCACCC		
UBA3	GAGCTGCTGGCTGAGAAAATG	CGCCAGCTCCAATGACTAGA		
UBA5	CGAATCCCTACAGCCGCTT	GCTACGGCAAAGGTACGGAT		
RAD50	GCGTGCGGAGTTTGAATA	TTGAGCAACCTTGGGATCGT		
SMARCE1	GCAGAAAGGTCTGGGACCAA	CAAGGTACGCGGGGAATTA		
CDK2	CCTGGACACTGAGACTGAGG	CAGTGAGAGCAGAGGCATCC		
CDK4	GAGCATCCCAATGTTGTCCG	TCAGATCCTTGATCGTTTCGGC		
Primers for ChIP-qPCR	Forward	Reverse		
CDK6	GAAACGGCCTCCGTTCTTCA	GCTGACCAGCAGTACGAATG		
RAD51	CCCCCGGCATAAAGTTTGA	GCTTTCAGAAATCCCGCCA	from doi: 10.1371/journal.pone.0052810	
BRCA1	TTTCGTATTCTGAGAGGCTGCTG	ATTATCTGTAATTCCTCGGCTT	from doi: 10.1371/journal.pone.0052810	

**Table S3. Crystallography Data Collection and Refinement Statistics**

	<b>MS645</b>	<b>MS660</b>
<b>Data collection</b>		
Space group	P 2 <sub>1</sub> 2 <sub>1</sub> 2 <sub>1</sub>	P 6 <sub>5</sub> 2 2
Cell dimensions		
a, b, c (Å)	54.00, 59.72, 95.62	87.54, 87.54, 172.30
α, β, γ (°)	90, 90, 90	90, 90, 120
Resolution (Å) (highest resolution shell)	50-1.46(1.49-1.46)	50-2.96(3.01-2.96)
Measured reflections	2,247,727	7,152,128
Unique reflections	50373	8745
Rmerge	4.4(91.4)	13.3(81.2)
I/σ	53.6(2.6)	16.6(2.2)
Completeness (%)	92.8(95.3)	99.8(98.5)
Redundancy	11.5(11.1)	9.7(9.2)
<b>Refinement</b>		
Resolution (Å)	37.32-1.46	42.42-2.96
No. reflections	50320	8677
Rwork/ Rfree(%)	14.1/17.6	24.3/28.5
No. atoms		
Protein	2167	2070
Compound	64	62
Water	350	7
B-factors (Å <sup>2</sup> )		
Protein	21.5	54.8
Compound	10.4	42.0
Water	33.8	37.7
RMSD		
Bond lengths (Å)	0.005	0.003
Bond angles (o)	1.417	1.209
Ramachandran plot % residues		
Favored	98.8	93.8
Allowed	1.2	5.4
Outlier	0.0	0.8